processes

MDPI

Article

Xylose Hydrogenation Promoted by Ru/SiO_2 Sol–Gel Catalyst: From Batch to Continuous Operation

Anna Barone [1], Benedetta Anna De Liso [1], Henrik Grénman [2], Kari Eränen [2], Francesco Taddeo [1], Claudio Imparato [3], Antonio Aronne [3], Vincenzo Russo [1,2,*], Martino Di Serio [1] and Tapio Salmi [2]

[1] Department of Chemical Sciences, University of Naples Federico II, Via Cintia, IT-80126 Naples, Italy; anna.barone@gmail.com (A.B.); benedetta.deliso@gmail.com (B.A.D.L.); francesco.taddeo@unina.it (F.T.); diserio@unina.it (M.D.S.)
[2] Laboratory of Industrial Chemistry and Reaction Engineering, Åbo Akademi, Henrikinkatu 2, FI-20500 Turku/Åbo, Finland; henrik.grenman@abo.fi (H.G.); kari.eranen@abo.fi (K.E.); tapio.salmi@abo.fi (T.S.)
[3] Department of Chemical, Materials and Production Engineering, University of Naples Federico II, Piazzale Tecchio 80, IT-80125 Naples, Italy; claudio.imparato@unina.it (C.I.); antonio.aronne@unina.it (A.A.)
* Correspondence: v.russo@unina.it

Abstract: Xylose is nowadays converted into xylitol, a popular special chemical sweetener. Xylitol can be used not only in the pharmaceutical and food industries, but also in cosmetics and synthetic resins because of its countless properties. Conventionally, xylitol is produced by slurry reactors operating in batch with dispersed or supported catalysts. Hydrogen is continuously fed to maintain a constant pressure. In this work, the kinetics of the reaction were investigated to find the optimal operating conditions to minimize the by-products obtained. Given the great performances shown by the new Ru/SiO_2 sol–gel derived catalyst in glucose hydrogenation, in this work the mentioned catalyst was tested in the hydrogenation of xylose to xylitol both in batch and in continuous production to prove its stability and activity.

Keywords: xylose hydrogenation; xylitol; catalysis; scale-up; kinetics

Citation: Barone, A.; De Liso, B.A.; Grénman, H.; Eränen, K.; Taddeo, F.; Imparato, C.; Aronne, A.; Russo, V.; Di Serio, M.; Salmi, T. Xylose Hydrogenation Promoted by Ru/SiO_2 Sol–Gel Catalyst: From Batch to Continuous Operation. *Processes* **2024**, *12*, 27. https://doi.org/10.3390/pr12010027

Academic Editor: Chiing-Chang Chen

Received: 16 November 2023
Revised: 11 December 2023
Accepted: 17 December 2023
Published: 21 December 2023

1. Introduction

Biomass is the oldest known source of energy and chemicals, and it is a renewable source. Among the other chemical sources, biomass is extremely promising because it is widespread and available at low price in many countries [1]. Over 200 value-added compounds can be derived from lignocellulosic biomass (hemicelluloses, cellulose, and lignin) using various methodologies [2]. As an example, xylose is an important product, which can be obtained by the hydrolysis of hemicellulose. Building blocks such as xylitol can be obtained from xylose. Xylitol, a sugar alcohol with sweetness comparable to sucrose, offers numerous advantages as a food additive. Among these, it does not undergo Maillard reaction, and it mitigates the risk of obesity, thanks to being quickly metabolized and converted into energy. Xylitol is commonly employed in confectionery or pharmaceutical product coatings and in the formulation of dietary supplements [3,4].

The anticariogenic properties of xylitol have significant commercial impact due to their contribution to preventing the growth of oral bacteria, reducing plaque formation [5]. Xylitol can be obtained from the catalytic hydrogenation of xylose in three-phase slurry batch reactors [5,6], in an aqueous environment. In this process, hydrogen at high pressures and temperatures is employed. To enhance hydrogen solubility in the liquid bulk, high hydrogen pressure is essential, while high temperatures significantly increase the hydrogenation rate [7]. Nevertheless, the highest hydrogenation temperature is limited by the stability of sugar molecules. A Rushton turbine impeller was employed to ensure effective dispersion of gas and a good mixing of the reactants. Vigorous stirring is required to overcome the

mass transfer resistances between gas–liquid and liquid–solid phases and finely dispersed catalyst particles are used to suppress the different resistance inside the catalyst pores. The catalysts generally used in this process are heterogeneous, based on active metals, such as Raney-Nickel catalysts [8]. Low price, high activity and selectivity are the main benefits connected with the use of these catalysts [9]. However, the principal drawback is their relatively rapid deactivation and leaching of the promoter, causing the poisoning of the active surface [10]. Recently, different supported metals have been proposed for hydrogenation processes. Among them, ruthenium-based materials emerged as an attractive alternative to Ni-based catalysts in hydrogenation reactions [11–13]. Co supported on commercially available silica allowed high yields of xylitol to be reached, managing to reuse the catalyst three times before significant deactivation occurred [14]. The supported Ni catalysts showed good stability and activity, but the selectivity towards xylitol was not exceptionally high in the case of catalysts derived from perovskite precursor [15], while in those derived from phyllosilicate precursor, the selectivity has proven to be superior [16]. Bimetallic Cu-Ni catalysts supported on silica were also employed at mild temperature and hydrogen pressure, demonstrating to be effective in xylose hydrogenation [17]. A comparison between different transition metals was made by Akpe et al. [18], revealing that higher activity was found with Ru followed by Rh-, Ni-, Pd- and Pt-based catalysts. Beyond the metal, the role of the support is fundamental in reactions conducted in the aqueous phase since water can lead to deactivation due to leaching or the collapse of the porous structure [19,20]. Vilcocq et al. studied the effect of different TiO_2 supports on the Ru-based catalyst in xylose hydrogenation [19], while in the work by Musci et al. [21], the effect of Ru supported on other materials, such as γ-alumina, zirconia, zirconia-alumina was investigated. The hydrogenation of both glucose and xylose was carried out, verifying that the activity of the catalysts was highly dependent on the surface metal dispersion.

In the hydrogenation mechanism (Figure 1) the carbonyl group of xylose is hydrogenated to obtain xylitol. The active catalyst (Ru-H) establishes a coordination bond with both the oxygen of the carbonyl and the α carbon of xylose. A nucleophilic addition of the hydride bond to the active metal (in the coordination sphere of the metal) occurs, in which the π bond is eliminated creating two new covalent bonds. An alkoxide ion is formed and protonated, resulting in the formation of a primary alcohol (xylitol) [8,22]. From an economical point of view, xylose hydrogenation is feasible at high temperatures and pressures: a relatively high temperature (T = 80–130 °C) is necessary to achieve a viable reaction rate. However, excessively high temperatures can produce undesirable by-products, such as the formation of xylulose through isomerization, which can be hydrogenated further to arabinitol and xylitol. Typical hydrogen pressures are 40–80 bar [23]. It has been observed that the activity and selectivity of ruthenium are largely variable depending on the support material. The Ru/C catalyst has been used for the hydrogenation of xylose, demonstrating effective performance [24,25]. As widely reported in the literature, the choice of the synthesis procedure can affect the interaction between the matrix and the metal and consequently the stability of the catalyst. The sol–gel process is a versatile bottom-up approach providing an alternative to prepare hybrid organic–inorganic mesostructured materials. This method allows a good mixing between the matrix and the active specie [26]. The advantages are low processing temperature, homogenous dispersion of the metal on the support, efficient immobilization of the active phase within the host matrix and high specific surface area. In a recent work [27], the $(RuO_2)_{0.038}(SiO_2)_{0.962}$ nanomaterial was synthesized by a one-pot sol–gel route from which a gel-derived catalyst (Ru/SiO_2) with a multimodal size distribution of the Ru nanoparticles in the silica matrix was obtained showing promising performance in terms of activity and selectivity for glucose hydrogenation to sorbitol. The aim of this work is to investigate the performance of the Ru/SiO_2 catalyst in selective xylose hydrogenation to xylitol under batch conditions, in comparison with a commercial Ru/C catalyst. The reaction kinetics was investigated in a series of systematic experiments. Finally, the Ru/SiO_2 catalyst was tested in a continuous reactor to verify the stability and check the influence of the main operation parameters on the activity and selectivity.

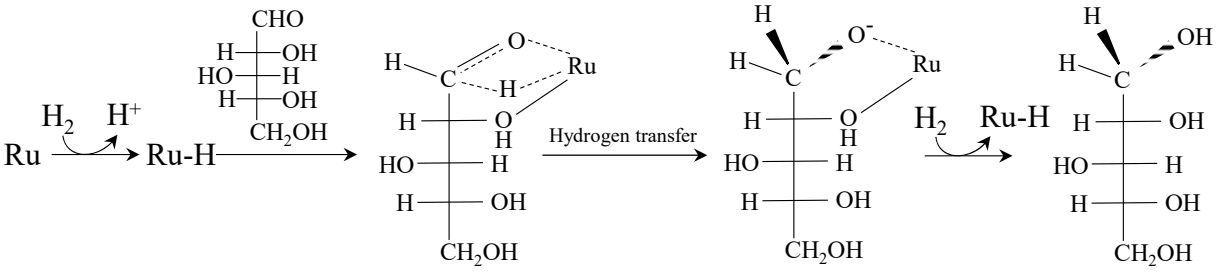

Figure 1. Reaction mechanism for xylose hydrogenation with Ru-based catalyst.

2. Materials and Methods

2.1. Materials

The Ru/SiO_2 catalyst was synthesized via sol–gel technique, based on the procedure developed in a previous publication [27], obtaining a molar composition $(RuO_2)_{0.038}(SiO_2)_{0.962}$, corresponding to 6.3 wt% of Ru in the reduced material. The precursors were $RuCl_3 \cdot 3H_2O$ (99.98 wt%) and $Si(OC_2H_5)_4$ (TEOS) (99 wt%). Ethanol and HCl (37 wt%) were used as solvent and catalyst, respectively. Briefly, a hydro-alcoholic solution of TEOS with a molar ratio of TEOS:EtOH:H_2O = 1:4:12 was prepared and stirred at room temperature. Subsequently, $RuCl_3 \cdot 3H_2O$ was added, followed by HCl (TEOS:HCl molar ratio = 1:0.15). A homogeneous gel was obtained within 2 weeks, then aged for 3 days and completely dried up to 383 K. Finally, the material was annealed in air flow at 773 K for 2 h in a tubular furnace.

2.2. Hydrogenation Experiment

2.2.1. Kinetic Studies in Batch Reactor

Experiments were conducted to reveal the kinetic behavior of xylose hydrogenation. The kinetic studies were made in a stainless steel (AISI 316) fed–batch reactor (Parr Instrument), where hydrogen was fed at constant pressure to a 0.3 L tank. The pressure was kept constant by controlled addition of hydrogen. The reactor scheme is shown in Figure 2A.

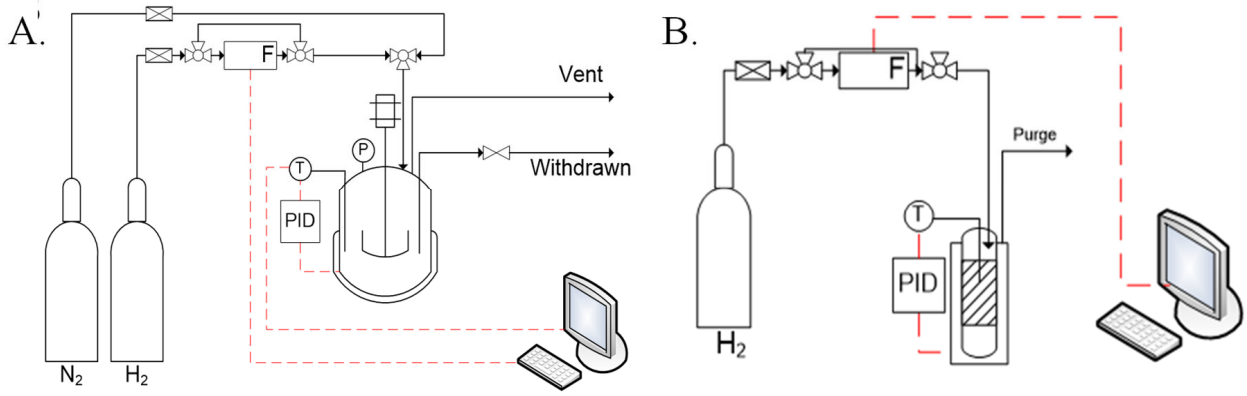

Figure 2. (**A**) Hydrogenation fed-batch reactor scheme. (**B**) Pre-reduction system scheme.

The reaction mixture composed of H_2O, sugar and catalyst was charged to the moveable vessel. The mixing in the reactor was achieved thanks to a gaseous effect produced at an optimized stirring speed (see results and discussion). The temperature was controlled by a rigid heating jacket connected to a thermoregulator, which allows the measurement of the temperature thanks to a thermocouple inside the reactor, and the hydrogen flow was set up by using a digital flowmeter. Firstly, the catalyst was pre–reduced to make it active, since metallic ruthenium is the active phase for hydrogenation. The system consists of a packed bed reactor operated at 0.1 L min^{-1} hydrogen flow, 1 bar and a fixed temperature of 573 K for 3 h (Figure 2B). A set of tests was conducted at different hydrogen pressures,

temperatures, catalyst amounts and xylose concentrations. The operation conditions of the experiments are listed in Table 1. The experimental method consists of charging the reactor with 200 g of the reactant solution and the catalyst. After flushing with nitrogen to evacuate dissolved oxygen, hydrogen was introduced into the reactor at the desired pressure, which represented the starting point of the reaction. The experiment was conducted for several hours and samples of 2–4 mL were withdrawn from the reactor vessel periodically, to evaluate both the sugar conversion and the alcohol selectivity. After the experiment, the catalyst was washed with distilled water and subsequently reused in other tests. Cycles of five experiments were performed, under the same experimental conditions, to evaluate the stability and the activity over a long duration of catalyst use.

Table 1. Summary of operation conditions of kinetic tests conducted in the fed-batch reactor. * Experiment repeated imposing stirring rates of 200, 400 and 750 rpm.

Test	T [K]	v [rpm]	ρ_B [kg/m^3]	$C_{xylose,0}$ [mol/m^3]	P_{N2} [bar]	P_{H2} [bar]
1 *	393	600	2.50	100	1	20
2	393	600	1.82	100	1	20
3	393	600	1.25	100	1	20
4	393	600	0.75	100	1	20
5	373	600	1.25	100	1	20
6	353	600	1.25	100	1	20
7	393	600	1.25	100	1	15
8	393	600	1.25	100	1	10
9	393	600	1.25	75	1	20

2.2.2. Continuous Hydrogenation Experiments

Catalyst stability experiments were performed in a continuous three-phase reactor displayed in Figure 3.

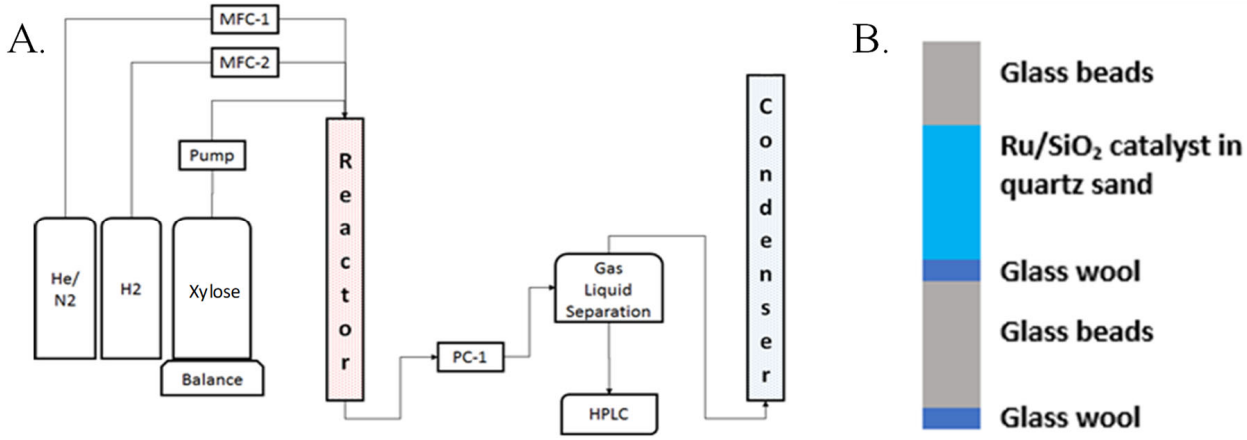

Figure 3. (**A**) Continuous reactor for hydrogenation. (**B**) Reactor tube filling.

The reactor set-up is made of a 50 cm long stainless-steel tube with an internal diameter of 4.2 mm. The reactor was filled by placing glass wool on the bottom to avoid the loss of components from the catalyst bed. After washing with acid, 4.5 g of glass beads (Sigma-Aldrich, Burlington, MA, USA) with diameters 450–600 µm, a second layer of glass wool, 3.3 g of quartz sands mixed with the catalyst and a final layer of glass beads were added to the tube. The reactor was operated in trickle-flow mode. A Brooks (5850S) mass flow controller was used to regulate the flow of the inert He/N_2 gas. The xylose solution was fed to the reactor through an Eldex HPLC pump, and the flow was checked placing the bottle on a balance. An electrical oven (ATS, 3210) and an Equilibar gas-liquid back pressure regulator allowed for the heating and control of the pressure of the system, respectively.

A 25 mL three-neck flask was employed to separate the gas-liquid flow coming from the pressure controller. One neck served as the inlet, another one allowed the gas to flow out, and the third was used for periodic liquid withdrawal. In order to dry the gases flowing from the gas-liquid separator, a condenser operating at −5 °C (LAUDA, RE106) was employed. The reaction conditions were screened by changing the temperature, catalyst amount, feed flow rate and concentration at a constant hydrogen flow rate (35 mL/min). The operation conditions adopted in the continuous experiments are reported in Table 2. The total hydrogen pressure in the system was maintained constant at 20 bar. To remove oxygen from the system, nitrogen flowed for 15 min before each experiment. The catalyst was reduced in situ under hydrogen flow at 1 bar and 573 K for 180 min. In order to eliminate oxygen and ensure the hydrogen saturation of the liquid phase, the feedstock was bubbled with hydrogen for 10 min before each test.

Table 2. Summary of operation conditions of continuous experiments (*).

Test	T [K]	$w_{Catalyst}$ [kg]	ρ_B [kg/m^3]	$C_{xylose,feed}$ [mol/m^3]	Q [m^3/s]	P_{H2} [bar]
1 *	393	0.2×10^{-3}	28.8	100	3.3×10^{-9}	20
2 *	373	0.2×10^{-3}	28.8	100	3.3×10^{-9}	20
3 *	353	0.2×10^{-3}	28.8	100	3.3×10^{-9}	20
4 *	373	0.2×10^{-3}	28.8	100	3.3×10^{-9}	20
5 *	373	0.2×10^{-3}	28.8	100	1.3×10^{-9}	20
6 *	373	0.1×10^{-3}	14.4	100	3.3×10^{-8}	20

2.2.3. Analytical Method

Two different HPLC devices were used for chemical analysis. High-performance liquid chromatography (HPLC) was used for the quantification of the reagent (xylose), product (xylitol) and the by–product (arabinitol) observed during xylose hydrogenation carried out in the fed-batch reactor. Resolution of reaction products was achieved by elution through the ion–exclusion column RCM-Monosaccharide Ca^{2+} (8%) by Phenomenex. The species were analyzed via Sedex ELSD (Evaporative Light Scattering Detection) at 313 K and 3 bar. Retentions times (xylose: 10.73 min; d-arabinitol: 17.57 min; xylitol: 20.76 min) and ELSD response factor for the species were determined by using commercial standards. The concentrations for the continuous hydrogenation experiments were determined through off-line analysis using HPLC (VWR HITACHI Chromaster). A Biorad Aminex HPX-87C carbohydrate was used as column with a refractive index (HP 1047A) as detector [28]. In the kinetic studies in the batch reactor only arabinitol was obtained as a by-product, but in the continuous experiments furfural and xylulose were also found in the samples. The retention times (xylose: 9.50 min; xylulose: 16.74 min; arabinitol: 18.83 min; xylitol: 22.74 min) and RI responses factor for the species were determined via comparison with commercial standards.

2.2.4. Catalyst Characterization

A JEOL 3010-UHR instrument operating at 300 kV, was used to obtain transmission electron microscopy (TEM) and high-resolution (HR)-TEM micrographs. The instrument was equipped with a LaB_6 filament and a Link ISIS 200 as detector for X-ray energy-dispersive spectroscopy analysis. Digital micrographs were acquired via a 2000 × 2000 pixel Gatan US1000 CCD camera. The samples were deposited as powders on a copper grid covered with a lacey carbon film. Histograms of the Ru particle size distribution were generated by considering a statistically representative number of particles from the HR-TEM images. The mean particle diameter (d_m) was then calculated as:

$$d_m = \sum d_i n_i / \sum n_i \quad (1)$$

Moreover, the Ru specific surface area of the supported metal particles (assumed to be spherical) was calculated based on the corresponding particle size distribution using Equation (2):

$$RuSSA = 3\sum n_i r_i^2 / \left(\rho_{Ru} \sum n_i r_i^3\right) \quad (2)$$

where r_i is the mean radius of the size class containing n_i particles, and ρ_{Ru} is the volumetric mass of Ru equal to 12.41 g·cm^{-3}. To evaluate the theoretical metal area (Ru SA), approximately 0.5 g of catalyst and the Ru loading of the Ru/C and Ru-SiO_2 catalysts (5.0 and 6.30 wt%, respectively) were considered in the catalytic tests.

N_2 isotherms were measured at −196 °C on approximately 100 mg of powder, previously outgassed at 300 °C for 3 h to remove water and other atmospheric contaminants (Quantachrome Autosorb 1 instrument). Specific surface area values of the powder were calculated according to the Brunauer–Emmett–Teller (BET) method.

3. Results and Discussion

3.1. Experiments in Batch Reactor

A set of experiments was performed by pre–reducing the Ru/SiO_2 catalyst at 573 K to compare its activity with that of a commercial Ru/C catalyst, typically used in xylose hydrogenation. Xylose conversion and xylitol selectivity were evaluated by performing reuse experiments after five cycles of 15 min (900 s) for Ru/C and for 5 cycles of 5 h (18,000 s) for Ru/SiO_2. The different reaction times were selected due to the different activities of the catalysts. The results are shown in Figure 4.

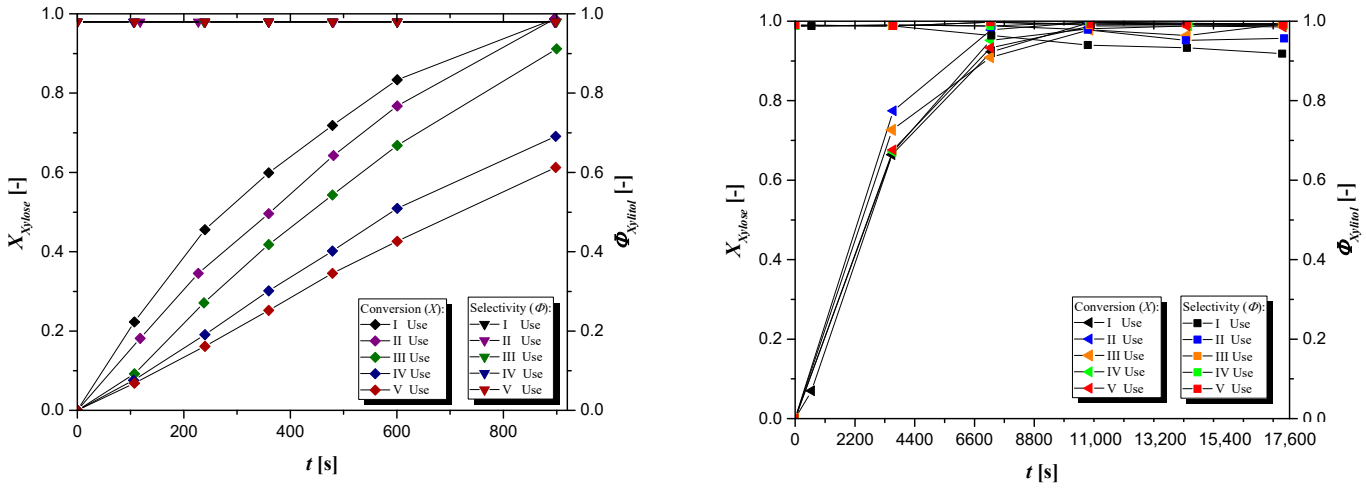

(**A**) (**B**)

Figure 4. (**A**) Xylose conversion and xylitol selectivity trends for each reuse cycle performed using Ru/C commercial catalyst. (**B**) Xylose conversion and xylitol selectivity trends for each reuse cycle performed using Ru/SiO_2 synthesis catalyst. Experiments were conducted fixing v = 600 rpm, T = 393 K, ρ_B = 2.50 kg/m^3, $C_{xylose,0}$ = 100 mol/m^3 and P_{H2} = 20 bar.

As already observed for glucose hydrogenation [27], the Ru/C catalyst showed high activity without a reduction of the selectivity (Figure 4A) but it deactivated rapidly. The performance of the two catalysts were compared in detail; conversion achieved in the first use of Ru/C at 600 s was 0.82, while it was 0.07 with the Ru/SiO_2 catalyst. The deactivation is really fast, already starting from the second cycle of use. Instead, after five cycles of 5 h, the Ru/SiO_2 catalyst activity remained constant. The same trend is shown for the selectivity, which did not change in successive experiments. The turnover frequency (TOF)

(Figure 5) was calculated to make a comparison between the two tested catalysts as the sugar consumption rate referred to the moles of ruthenium.

$$TOF = -\frac{1}{n_{Ru}} \frac{dn_{sugar}}{dt} \quad (3)$$

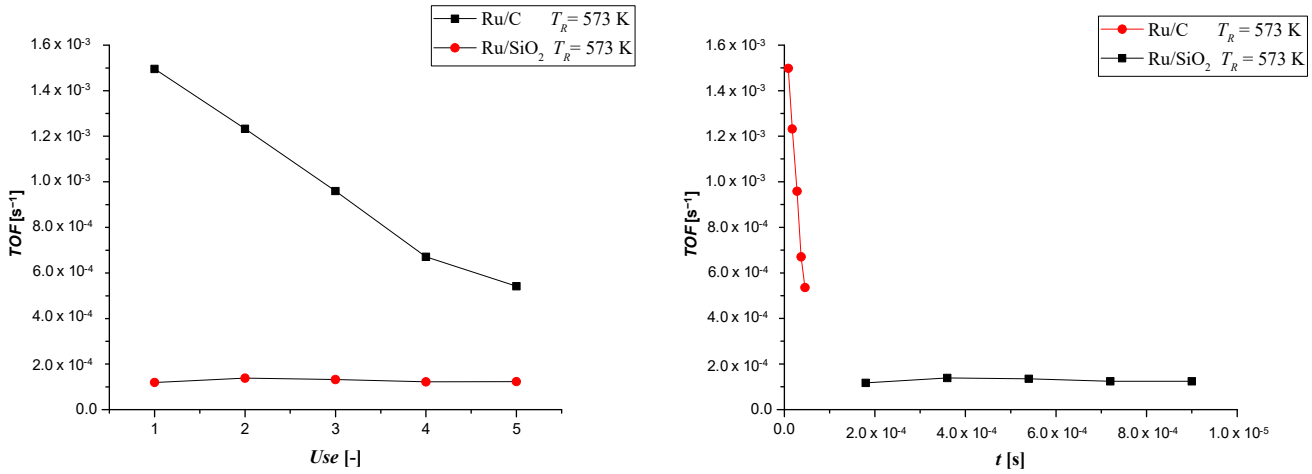

Figure 5. TOF trend for each catalyst tested in the xylose hydrogenation as a function of (**A**) reuse cycles and (**B**) cumulative time. Experiments were conducted fixing v = 600 rpm, T = 393 K, ρ_B = 2.50 kg/m^3, $C_{xylose,0}$ = 100 mol/m^3 and P_{H2} = 20 bar.

As evidenced in Figure 5A,B, where TOF is plotted against cycles of use and time, respectively, a high activity is shown by Ru/C in the first cycle, then it rapidly decreases in only 75 min (4500 s) of reaction. In contrast, Ru/SiO_2 shows no activity loss, and its TOF seems to be constant in 25 h (90,000 s) of reaction. This remarkable catalytic stability can be attributed to the fine dispersion of small Ru nanoparticles and their effective interaction with the silica matrix, resulting from the adopted sol–gel synthesis route, as previously demonstrated [27].

Different experiments were conducted in the stirring rate of the system, to verify the influence of eventual diffusion limitations, both gas-liquid and liquid-solid. The trend of the observed reaction rate vs. the stirring rate of the system is reported in Figure 6.

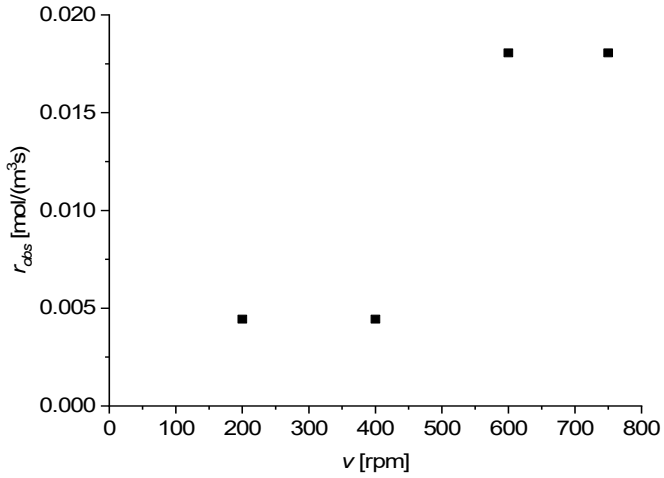

Figure 6. Influence of the stirring rate of the system on the observed reaction rate. Experiments were conducted fixing, T = 393 K, ρ_B = 2.50 kg/m^3, $C_{xylose,0}$ = 100 mol/m^3 and P_{H2} = 20 bar.

As revealed, from v = 600 rpm, the observed rate does not change anymore, demonstrating that neither gas-liquid nor liquid-solid diffusion limitations are dominant.

The eventual influence of intraparticle diffusion limitations were checked by applying the Weisz-Prater criterion [29]. The criterion gave, in every case, a value lower than three, indicating possible concentration gradients inside the catalyst.

Tests were performed with different Ru/SiO_2 amounts, expressed in terms of bulk density, to investigate the effect of this parameter on the reaction rate. The xylose conversion and xylitol selectivity trends are shown below in Figure 7.

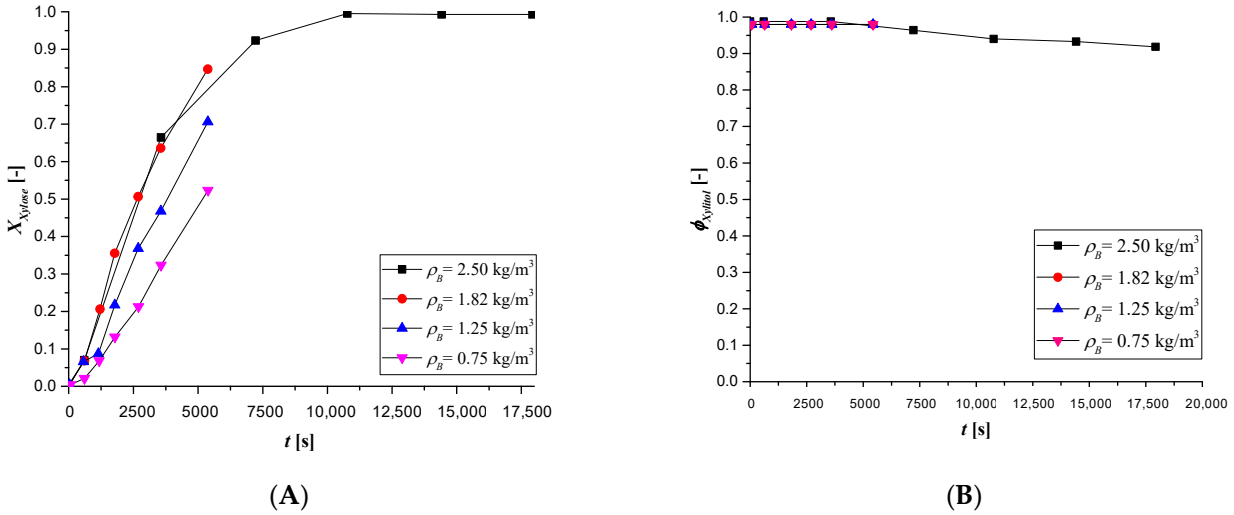

(**A**) (**B**)

Figure 7. (**A**) Xylose conversion and (**B**) xylitol selectivity trend for different bulk densities of Ru/SiO_2 catalyst. Experiments were conducted fixing v = 600 rpm, T = 393 K, $C_{xylose,0}$ = 100 mol/m^3 and P_{H2} = 20 bar.

It is evident from Figure 7A that the reaction rate increases with the amount of catalyst loading, while Figure 7B shows almost the same selectivity at the highest catalyst amount. Using an excessive catalyst loading, secondary reactions can be promoted leading to by-products generation (i.e., arabitol, xylulose). Plotting the conversion of xylose against the normalized reaction time for the bulk density of the catalyst confirms that the experimental data overlap (Figure 8). This implies that the reaction kinetics are linearly dependent on the catalyst bulk density, indicating that the experiments were conducted within the regime of intrinsic kinetics.

The temperature was varied in a range between 353 K and 393 K to evaluate the effect on the hydrogenation reaction, as reported in Table 1. The results, in terms of conversion achieved at 180 min, are shown in Figure 9, where it is possible to see that the xylose conversion increases gradually in the investigated temperature range.

Plotting the logarithm of the rate constant, k, obtained by the observed reaction rate fixing a first order reaction rate, versus the reverse of the temperature, $1/T$, it is possible to see that the experimental data follow an Arrhenius behavior (Figure 9). According to the linearized Arrhenius equation, the apparent activation energy is equal to 70 $\pm$ 1 kJ/mol. A set of experiments was carried out to investigate the effect of hydrogen pressure on the reaction kinetics. The results shown in Figure 10 confirm that by changing the pressure from 10 bar to 15 bar the conversion increases by 20%, but by increasing the pressure no further increase in the conversion can be seen suggesting that the active sites are saturated by the hydrogen molecules, limiting the adsorption of further reagent molecules. This has a positive effect on the selectivity because it avoids the formation of by-products; on the other hand, it has limiting effects on xylose conversion. The autocatalytic trend observed could be justified by a progressively deeper catalyst reduction during the hydrogenation reaction, leading to the formation of new active sites.

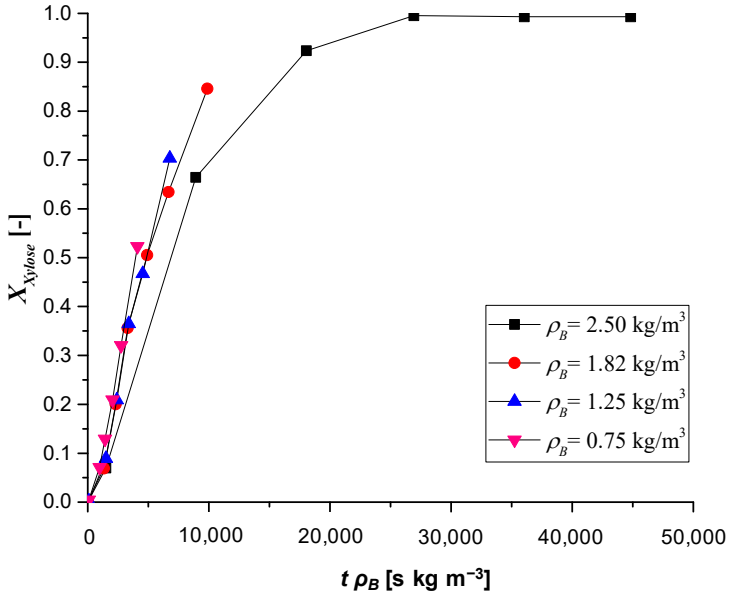

Figure 8. Xylose conversion trend for different bulk density of Ru/SiO_2 catalyst. Experiments were conducted fixing v = 600 rpm, T = 393 K, $C_{xylose,0}$ = 100 mol/m^3 and P_{H2} = 20 bar.

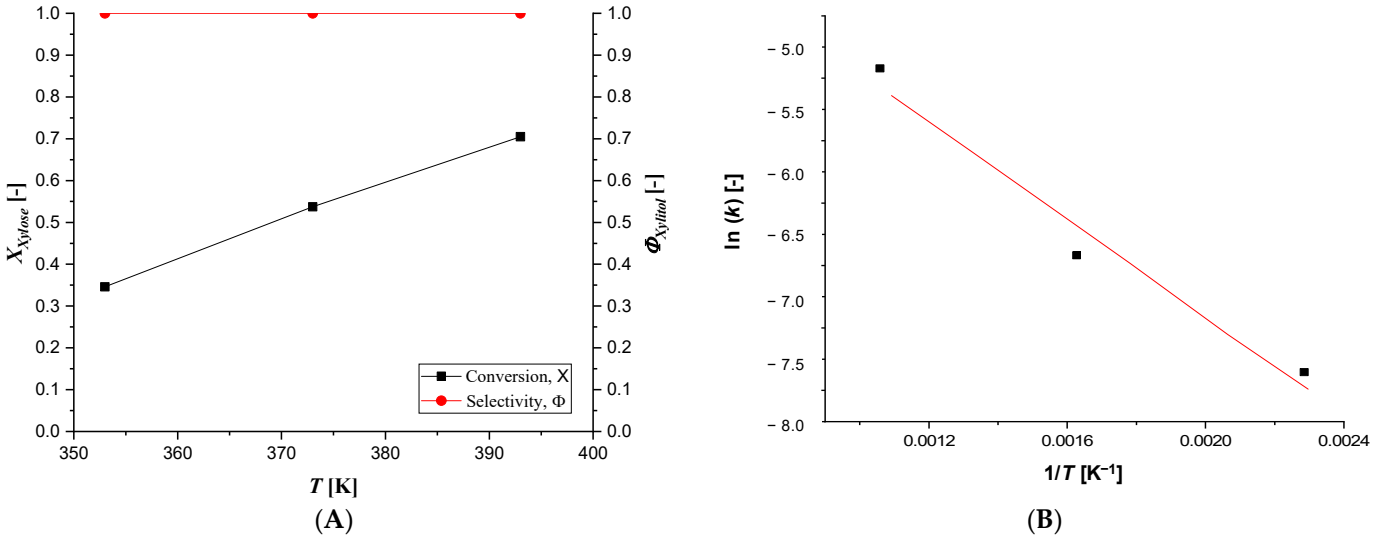

Figure 9. (**A**) Temperature effect on the conversion of xylose and the selectivity to xylitol. (**B**) Arrhenius behavior of experimental data. Experiments were conducted fixing v = 600 rpm, ρ_B = 2.50 kg/m^3, $C_{xylose,0}$ = 100 mol/m^3 and P_{H2} = 20 bar.

Experiments at two different initial concentrations, namely 75 mol/m^3 and 100 mol/m^3, were conducted to study the influence of xylose concentration.

The results in Figure 11 show that with a solution of 75 mol/m^3, the conversion of xylose and the selectivity to xylitol are higher than the values obtained with a concentration of 100 mol/m^3, likely because the strong adsorption of xylose molecules during the hydrogenation reaction has a retarding effect. This fact was further elaborated on by calculating the space time yields for the two experiments, obtaining 0.013 and 0.011 mol/(m^3 s) when using, respectively, 100 and 75 mol/m^3 as initial xylose concentrations, indicating that a similar space time yield is obtained by increasing the reactant concentration. Thus, it is possible to conclude that the reactant shows an inhibition behavior towards the reaction rate. The observation that the increase in the reactant concentration inhibits product formation is quite surprising. However, this phenomenon is rather common in biological reactions [30].

For example, when an enzyme, like amylase in the hydrolysis of starch into glucose, is used as a catalyst, a higher concentration of starch reduces the product formation. This is because starch molecules block the active sites of the enzymes and prevent the occurrence of the reaction. The same reason may explain the diminished product (xylitol) formation with the increasing concentrations of reactant (xylose). A higher concentration of xylose itself does not allow other molecules of xylose to come in contact with hydrogen gas on the surface of Ru active sites.

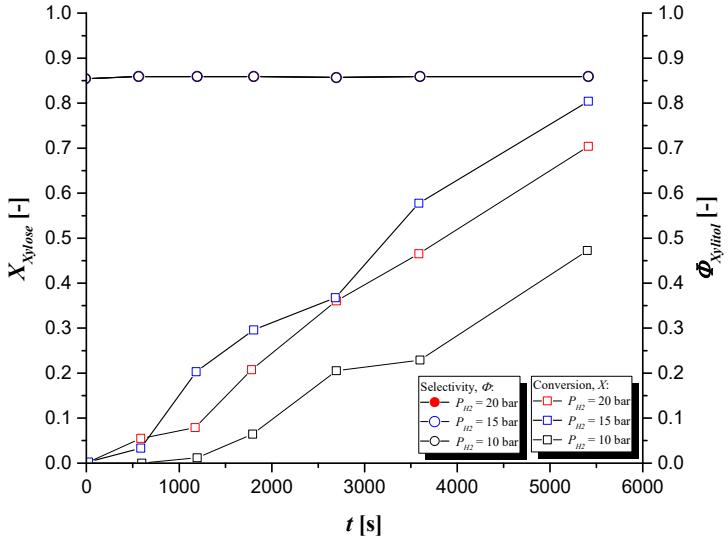

Figure 10. Effect of hydrogen pressure on xylose conversion and xylitol selectivity. Experiments were conducted fixing v = 600 rpm, T = 393 K, ρ_B = 2.50 kg/m^3 and $C_{xylose,0}$ = 100 mol/m^3.

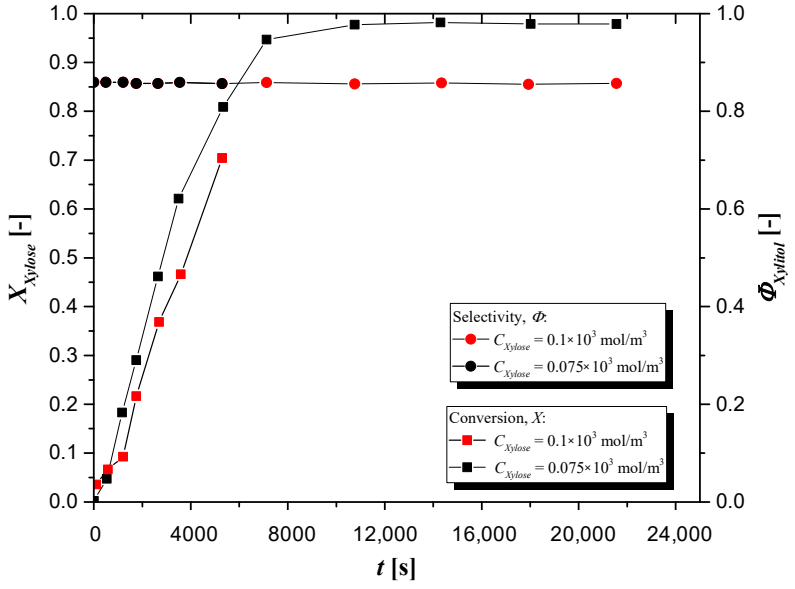

Figure 11. Effect of xylose concentration on xylose conversion and xylitol selectivity. Experiments were conducted fixing v = 600 rpm, T = 393 K, ρ_B = 2.50 kg/m^3 and P_{H2} = 20 bar.

3.2. Experiments in Continuous Packed Bed Reactor

To study the performance of the Ru/SiO_2 catalyst, a long-term test of 48 h (172,800 s) was conducted, investigating its stability in terms of xylose conversion and xylitol selectivity (see Figure 12).

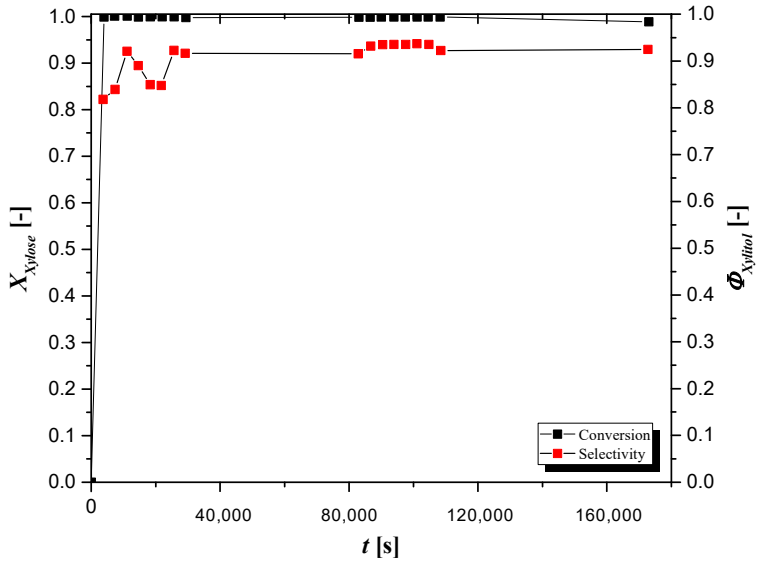

Figure 12. Xylose conversion and xylitol selectivity trend for 48 h of reaction. Experiments were conducted fixing T = 373 K, ρ_B = 28.8 kg/m^3, $C_{xylose,feed}$ = 100 mol/m^3, Q = 3.3 × 10^{-9} m^3/s and P_{H2} = 20 bar.

The results clearly show that the catalyst is very stable for the whole experiment, in fact, the selectivity and the conversion remained constant. These results are in line with what was observed in batch conditions in the reuse experiments (see Figure 4B).

This observation is supported by the information obtained from TEM images where the Ru distribution stayed invariant with respect to the original catalyst after several hours of reaction, confirming that Ru nanoparticles are effectively stabilized through interaction with the SiO_2 support, due to the synthesis procedure used [27]. A set of tests were conducted to study the effect of temperature.

According to the results obtained in batch operation, the reaction is strongly influenced by temperature. Figure 13A shows the positive effect of the temperature on conversion, which is the highest (100%) at 393 K, while Figure 13B confirms the negative effect on selectivity since, as previously shown, the solubility of the hydrogen decreases. Moreover, the highest formation of by-product was observed under the more severe conditions of temperature (373 K and 393 K), contributing to the decrease in xylose selectivity. By calculating the xylitol productivity as moles of xylitol formed per gram of ruthenium and per minute, and plotting it versus reaction time, it is possible to see better the temperature effect.

It is clear, from the results reported in Figure 14, that at 353 K the productivity in the first two hours of reaction decreases while it increases at 373 K and 393 K. It is possible to estimate an average value of productivity around 0.031 mol/(s kg). Figure 15 confirms that the xylose conversion and the xylitol selectivity are correlated with residence time, which can be improved by increasing the size of the catalyst bed. The negative effect of the liquid flow rate on the conversion suggests operations under non-optimal residence times: at higher liquid flow rates, the residence time is at its shortest. The opposite trend is obtained for the selectivity on which the liquid flow rate has a positive effect. This is because in a short residence time only a small amount of by-products (e.g., arabitol, xylulose) manage to form. This behavior is visible by plotting the conversion of xylose and selectivity to xylitol as a function of the WHSV (Weight Hourly Space Velocity). WHSV is defined as the feed flowing weight per unit of the catalyst per hour. Since the weight of the catalyst in the reactor remains constant, any variation in the flow of liquid per hour will change the WHSV. The inverse of the space velocity is the contact time, representing the time of contact between the liquid and the catalyst under the operation conditions.

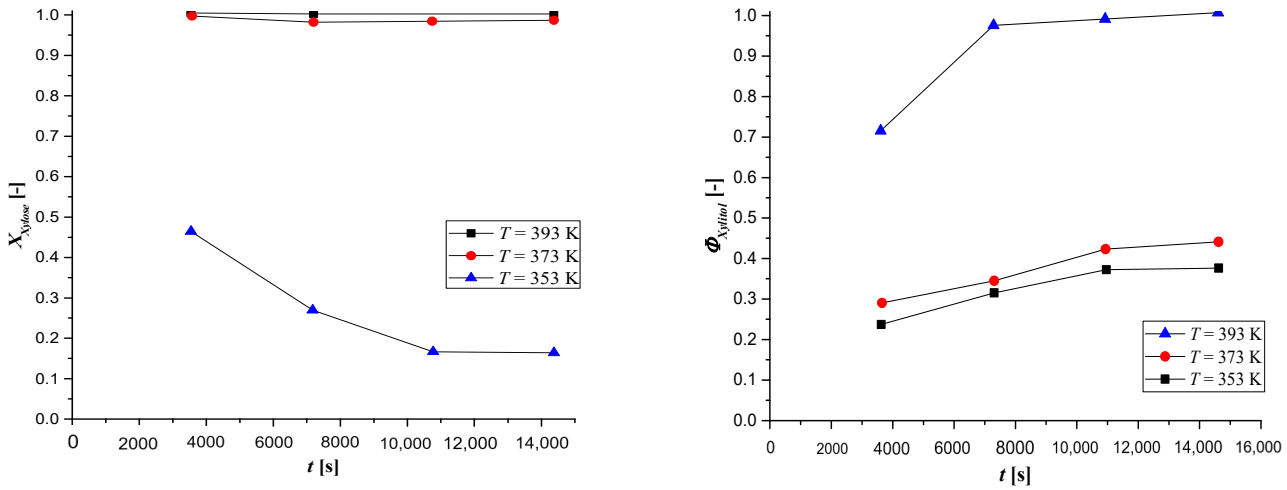

(A) **(B)**

Figure 13. Effect of temperature: (**A**) on xylose conversion and (**B**) on xylitol selectivity. Experiments were conducted fixing ρ_B = 28.8 kg/m^3, $C_{xylose,feed}$ = 100 mol/m^3, Q = 3.3 × 10^{-9} m^3/s and P_{H2} = 20 bar.

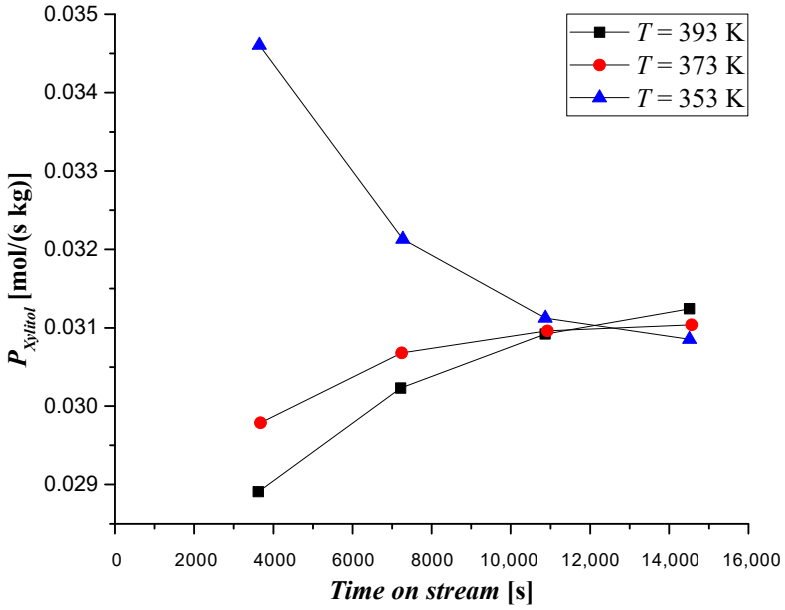

Figure 14. Effect of temperature on xylitol productivity. Experiments were conducted fixing ρ_B = 28.8 kg/m^3, $C_{xylose,feed}$ = 100 mol/m^3, Q = 3.3 × 10^{-9} m^3/s and P_{H2} = 20 bar.

The effect of catalyst weight was studied as well. It is seen from Figure 16 that 65% of conversion is obtained with 1 × 10^{-4} kg, which reaches almost full conversion, doubling the catalyst loading.

The effect is the opposite for the selectivity that is lower in correspondence with the highest amount of catalyst due to the increase in the amount of by-products.

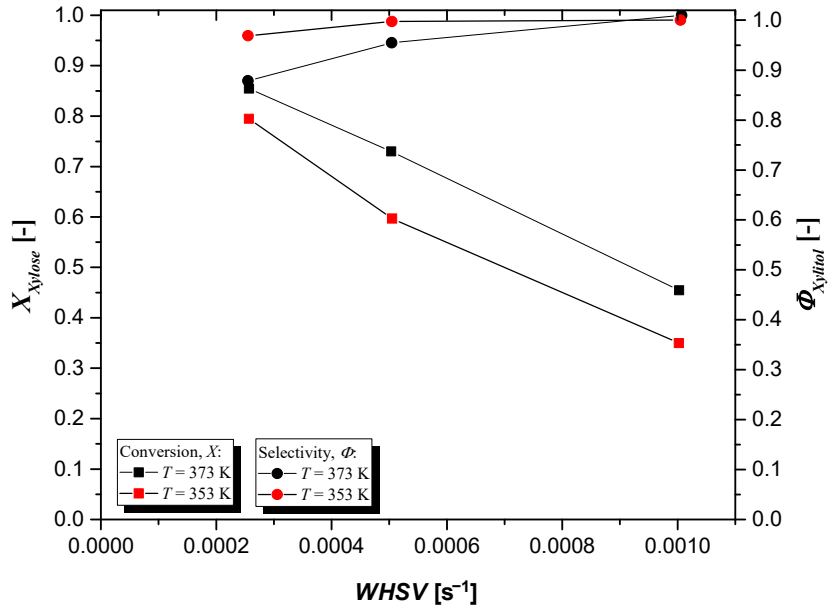

Figure 15. Xylose conversion and xylitol selectivity against WHSV at different temperatures. Experiments were conducted fixing ρ_B = 28.8 kg/m^3, $C_{xylose,feed}$ = 100 mol/m^3 and P_{H2} = 20 bar.

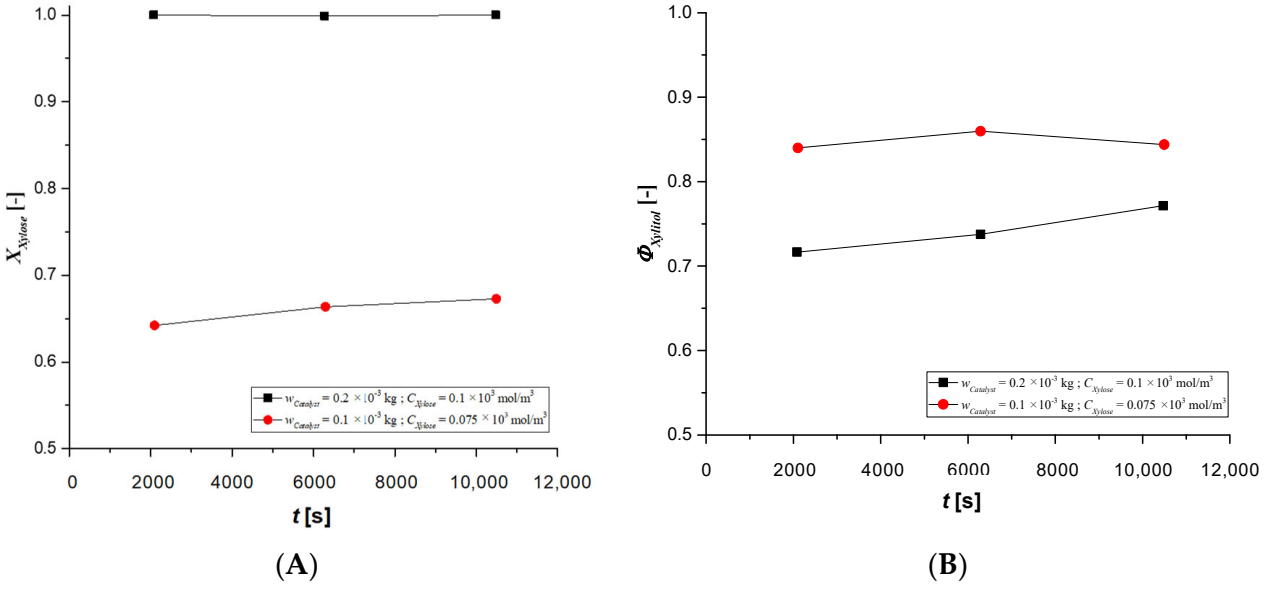

(**A**) (**B**)

Figure 16. Effect of catalyst amount: (**A**) on xylose conversion and (**B**) xylitol selectivity. Experiments were conducted fixing T = 373 K, $C_{xylose,feed}$ = 100 mol/m^3, Q = 3.3 × 10^{-9} m^3/s and P_{H2} = 20 bar.

3.3. Catalyst Characterization Results

TEM images of the catalysts and of the catalysts after reuse cycles are displayed in Figure 17, displaying no significant change in the catalyst after reuse.

After 25 h of reaction, Ru nanoparticle cluster dimensions did not vary significantly, further demonstrating the stability of the material (Figure 18).

Ru SSA does not vary much after the five cycles, indicating that the Ru nanoparticles are fairly stabilized by the interaction with the SiO_2 support (see Table 3).

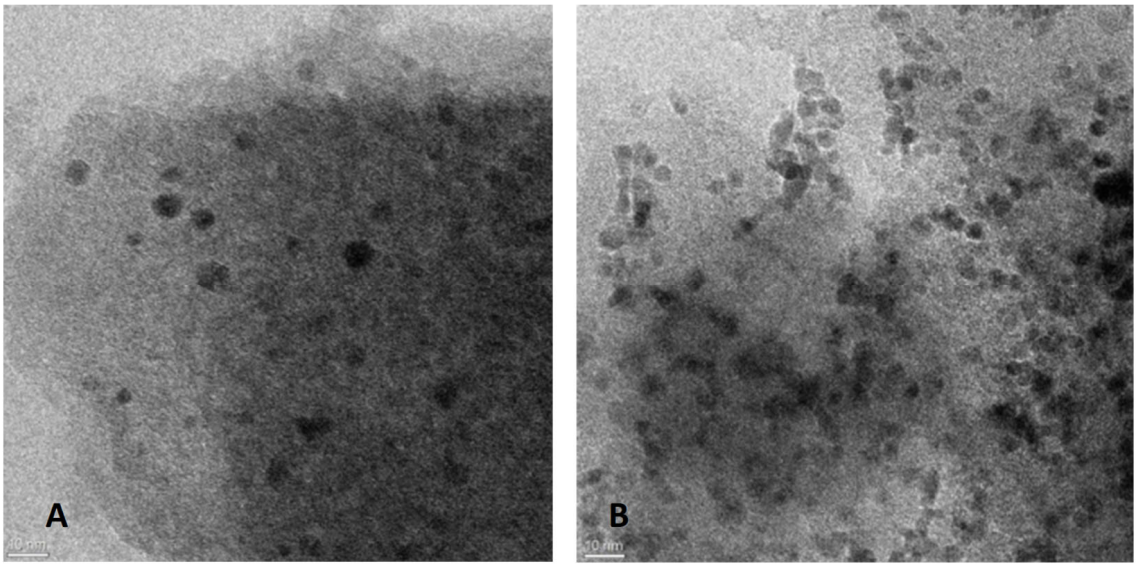

Figure 17. High magnification TEM images: (**A**) Ru/SiO_2 catalyst unused and (**B**) Ru/SiO_2 catalyst after five cycles of reaction.

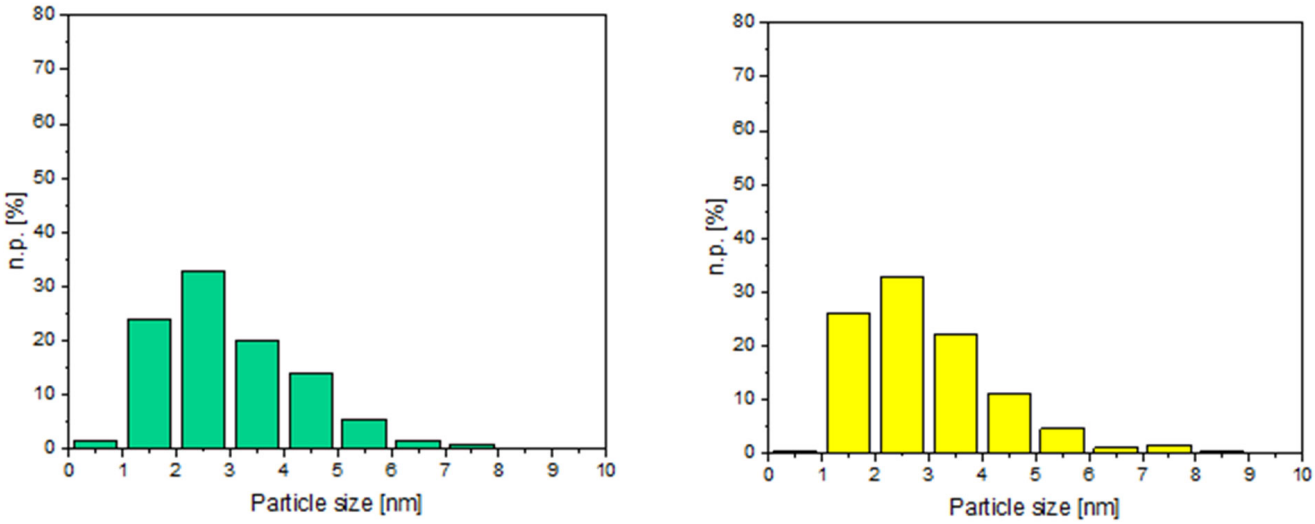

Figure 18. The average diameter of Ru nanocrystals distribution: (**A**) Ru/SiO_2 unused catalyst and (**B**) Ru/SiO_2 catalyst after 25 h of reaction.

Table 3. Ru Average Size (nm), metal SSA (m^2/g), and SA (m^2) using TEM analysis and BET SSA (m^2/g) using N_2 adsorption/desorption isotherms at −196 °C for Ru-SiO_2 catalysts.

Catalyst	Ru Average	Ru SSA	Ru SA [a]	BET SSA
Ru/SiO_2	2.9 ± 0.1	57.8	1.8	523
$Ru/SiO_{2(after\ 5\ cycles)}$	3.2 ± 0.1	53.8	1.8	580

[a] Calculated basing on the amount of catalyst used (ca. 0.5 g) and 6.30 wt % (Ru-SiO_2).

4. Conclusions

The hydrogenation of xylose was successfully made on a sol–gel derived Ru/SiO_2 catalyst in both a fed-batch and a continuous reactor. A series of batch experiments were carried out to determine the kinetic behavior of the reaction, investigating the effect of temperature, catalyst weight, hydrogen pressure and xylose concentration. The reusability

tests showed that the catalyst was very stable for five reaction cycles of 5 h. By analyzing the data obtained at different catalyst amounts it was verified that the reaction rate is of the first order with respect to the catalyst bulk density. The reaction rate became faster as the temperature increased. The apparent activation energy was estimated as 70 ± 1 kJ/mol, which is in agreement with values reported in the literature. The high selectivity of the Ru/SiO_2 was demonstrated as in most of the adopted conditions the main by-product (arabitol) yields were less than 1%. The stability and the activity of the synthesized catalyst were demonstrated in a continuous three-phase reactor. Long-term stability testing was performed, finding that Ru/SiO_2 was able to promote xylose hydrogenation for more than 40 h without any pronounced deactivation. Several reaction parameters, such as temperature, flow rate, catalyst amount and xylose concentration were screened to find suitable operative conditions.

Author Contributions: Conceptualization, V.R., M.D.S. and T.S.; methodology, K.E., C.I. and A.A.; formal analysis, F.T. and V.R.; investigation, A.B. and B.A.D.L.; data curation, A.B. and F.T.; writing—original draft preparation, A.B. and B.A.D.L.; writing—review and editing, H.G., F.T. and C.I.; supervision, H.G. and V.R.; project administration, V.R., M.D.S. and T.S.; funding acquisition, M.D.S. and T.S. All authors have read and agreed to the published version of the manuscript.

Funding: This research received no external funding.

Data Availability Statement: No data is available from the authors.

Acknowledgments: Luca Carnevale and Gaia Bottiglieri are kindly acknowledged for the experimental support in conducting some of the experiments in batch. C. Imparato acknowledges the support of the Agritech National Research Center, funded by the European Union Next-GenerationEU (Piano Nazionale di Ripresa e Resilienza (PNRR)—Missione 4 Componente 2, Investimento 1.4—D.D. 1032 17/06/2022, CN00000022). This manuscript reflects only the authors' views and opinions, neither the European Union nor the European Commission can be considered responsible for them.

Conflicts of Interest: Authors state no conflict of interest.

Nomenclature

C_{xylose}	Xylose concentration, mol/m^3
d_i	Particles diameter, m
d_m	Mean particle diameter, m
n	Amount of substance, mol
n_i	Number of particles
P	Pressure, bar
Q	Volumetric flowrate, m^3/s
r_i	Mean radius, m
r_{obs}	Observed reaction rate, mol/(m^3·s)
SA	Surface area, m^2
SSA	Specific surface area, m^2·g^{-1}
t	Time, min
T	Temperature, K
w	Mass, kg
X	Conversion, -
$P_{Xylitol}$	Productivity, mol/(s·kg)
Greek Symbols	
ρ_B	Catalyst bulk density, kg/m^3
ρ_{Ru}	Volumetric mass of Ru equal to 12.41 g/cm^3, g/cm^3
v	Stirring rate, rpm
Φ	Selectivity, -

Abbreviations

0	Initial condition
BET	Brunauer–Emmett– Teller
Feed	Feed conditions
HR-TEM	High-resolution transmission electron microscopy
TEM	Transmission electron microscopy
TOF	Turn-over frequency
WHSV	Weight hourly space velocity

References

1. Demirbaş, A. Biomass resource facilities and biomass conversion processing for fuels and chemicals. *Energy Convers. Manag.* **2001**, *42*, 1357–1378. [CrossRef]
2. Arena, B.J.; Allenza, P. Monosaccharides from Corn Kernel Hulls by Hydrolysis. U.S. Patent 475257, 21 June 1988.
3. Parajó, J.C.; Domínguez, H.; Domínguez, J.M. Biotechnological production of xylitol. Part 2: Operation in culture media made with commercial sugars. *Bioresour. Technol.* **1998**, *65*, 203–212. [CrossRef]
4. Zhang, J.; Zhang, B.; Wang, D.; Gao, X.; Hong, J. Xylitol production at high temperature by engineered Kluyveromyces marxianus. *Bioresour. Technol.* **2014**, *152*, 192–201. [CrossRef] [PubMed]
5. Rekola, M. Correlation between caries incidence and frequency of chewing gum sweetened with sucrose or xylitol. *Proc. Finn. Dent. Soc. Suom. Hammaslaakariseuran Toim.* **1989**, *85*, 21–24.
6. Yadav, M.; Mishra, D.K.; Hwang, J.S. Catalytic hydrogenation of xylose to xylitol using ruthenium catalyst on NiO modified TiO_2 support. *Appl. Catal. A Gen.* **2012**, *425–426*, 110–116. [CrossRef]
7. Pham, T.N.; Samikannu, A.; Rautio, A.R.; Juhasz, K.L.; Konya, Z.; Wärnå, J.; Kordas, K.; Mikkola, J.P. Catalytic Hydrogenation of d-Xylose Over Ru Decorated Carbon Foam Catalyst in a SpinChem®Rotating Bed Reactor. *Top. Catal.* **2016**, *59*, 1165–1177. [CrossRef]
8. Mikkola, J.P.; Sjöholm, R.; Salmi, T.; Mäki-Arvela, P. Xylose hydrogenation: Kinetic and NMR studies of the reaction mechanisms. *Catal. Today.* **1999**, *48*, 73–81. [CrossRef]
9. Sun, Z.; Zhang, Z.H.; Yuan, T.Q.; Ren, X.; Rong, Z. Raney Ni as a Versatile Catalyst for Biomass Conversion. *ACS Catal.* **2021**, *11*, 10508–10536. [CrossRef]
10. Hoffer, B.W.; Crezee, E.; Mooijman, P.R.M.; Van Langeveld, A.D.; Kapteijn, F.; Moulijn, J.A. Carbon supported Ru catalysts as promising alternative for Raney-type Ni in the selective hydrogenation of d-glucose. *Catal. Today* **2003**, *79–80*, 35–41. [CrossRef]
11. Freitas, V.D.S.; Paez, A.; Fongarland, P.; Philippe, R.; Vilcocq, L. Catalytic Hydrogenation of Hemicellulosic Sugars: Reaction Kinetics and Influence of Sugar Structure on Reaction Rate. *ChemCatChem* **2023**, *15*, e202300263. [CrossRef]
12. Zhang, X.J.; Li, H.W.; Bin, W.; Dou, B.J.; Chen, D.S.; Cheng, X.P.; Li, M.; Wang, H.Y.; Chen, K.Q.; Jin, L.Q.; et al. Efficient Synthesis of Sugar Alcohols under Mild Conditions Using a Novel Sugar-Selective Hydrogenation Catalyst Based on Ruthenium Valence Regulation. *J. Agric. Food Chem.* **2020**, *68*, 12393–12399. [CrossRef] [PubMed]
13. Bonnin, I.; Méreau, R.; Tassaing, T.; Jérôme, F.; De Oliveira Vigier, K. Hydrogenation of Sugars to Sugar Alcohols in the Presence of a Recyclable Ru/Al_2O_3 Catalyst Commercially Available. *ACS Sustain. Chem. Eng.* **2021**, *9*, 9240–9247. [CrossRef]
14. Audemar, M.; Ramdani, W.; Junhui, T.; Ifrim, A.R.; Ungureanu, A.; Jérôme, F.; Royer, S.; de Oliveira Vigier, K. Selective Hydrogenation of Xylose to Xylitol over Co/SiO_2 Catalysts. *ChemCatChem* **2020**, *12*, 1973–1978. [CrossRef]
15. Morales, R.; Campos, C.H.; Fierro, J.L.G.; Fraga, M.A.; Pecchi, G. Stable reduced Ni catalysts for xylose hydrogenation in aqueous medium. *Catal. Today* **2018**, *310*, 59–67. [CrossRef]
16. Du, H.; Ma, X.; Jiang, M.; Yan, P.; Zhao, Y.; Conrad Zhang, Z. Efficient Ni/SiO_2 catalyst derived from nickel phyllosilicate for xylose hydrogenation to xylitol. *Catal. Today* **2021**, *365*, 265–273. [CrossRef]
17. Du, H.; Ma, X.; Jiang, M.; Zhao, S.; Fang, Q.; Liu, X.; Zhang, Z.C. Xylitol Production from Xylose by Catalytic Hydrogenation over an Efficient Cu–Ni/SiO_2 Bimetallic Catalyst. *ACS Sustain. Chem. Eng.* **2023**, *11*, 2115–2126. [CrossRef]
18. Akpe, S.G.; Choi, S.H.; Ham, H.C. Conversion of cyclic xylose into xylitol on Ru, Pt, Pd, Ni, and Rh catalysts: A density functional theory study. *Phys. Chem. Chem. Phys.* **2021**, *23*, 26195–26208. [CrossRef]
19. Vilcocq, L.; Paez, A.; Freitas, V.D.S.; Veyre, L.; Fongarland, P.; Philippe, R. Unexpected reactivity related to support effects during xylose hydrogenation over ruthenium catalysts. *RSC Adv.* **2021**, *11*, 39387–39398. [CrossRef]
20. Hernandez-Mejia, C.; Gnanakumar, E.S.; Olivos-Suarez, A.; Gascon, J.; Greer, H.F.; Zhou, W.; Rothenberg, G.; Shiju, N.R. Ru/TiO_2-catalysed hydrogenation of xylose: The role of the crystal structure of the support. *Catal. Sci. Technol.* **2016**, *6*, 577–582. [CrossRef]
21. Musci, J.J.; Montaña, M.; Rodríguez-Castellón, E.; Lick, I.D.; Casella, M.L. Selective aqueous-phase hydrogenation of glucose and xylose over ruthenium-based catalysts: Influence of the support. *Mol. Catal.* **2020**, *495*, 111150. [CrossRef]
22. Delgado Arcaño, Y.; Valmaña García, O.D.; Mandelli, D.; Carvalho, W.A.; Magalhães Pontes, L.A. Xylitol: A review on the progress and challenges of its production by chemical route. *Catal. Today* **2020**, *344*, 2–14. [CrossRef]
23. Mikkola, J.P.; Salmi, T.; Sjöholm, R. Effects of solvent polarity on the hydrogenation of xylose. *J. Chem. Technol. Biotechnol.* **2001**, *76*, 90–100. [CrossRef]

24. Baudel, H.M.; de Abreu, C.A.M.; Zaror, C.Z. Xylitol production via catalytic hydrogenation of sugarcane bagasse dissolving pulp liquid effluents over Ru/C catalyst. *J. Chem. Technol. Biotechnol.* **2005**, *80*, 230–233. [CrossRef]
25. Sifontes Herrera, V.A.; Oladele, O.; Kordás, K.; Eränen, K.; Mikkola, J.P.; Murzin, D.Y.; Salmi, T. Sugar hydrogenation over a Ru/C catalyst. *J. Chem. Technol. Biotechnol.* **2011**, *86*, 658–668. [CrossRef]
26. Gonzalez, R.D.; Lopez, T.; Gomez, R. Sol-gel preparation of supported metal catalysts. *Catal. Today* **1997**, *35*, 293–317. [CrossRef]
27. Esposito, S.; Silvestri, B.; Russo, V.; Bonelli, B.; Manzoli, M.; Deorsola, F.A.; Vergara, A.; Aronne, A.; Di Serio, M. Self-Activating Catalyst for Glucose Hydrogenation in the Aqueous Phase under Mild Conditions. *ACS Catal.* **2019**, *9*, 3426–3436. [CrossRef]
28. Simms, P.J.; Hicks, K.B.; Haines, R.M.; Hotchkiss, A.T.; Osman, S.F. Separation of lactose, lactobionic acid and lactobionolactone by high-performance liquid chromatography. *J. Chromatogr. A* **1994**, *667*, 67–73. [CrossRef]
29. Jess, A.; Wasserscheid, P. *Chemical Technology: An Integral Textbook*; Wiley-Vch: Weinheim, Germany, 2013.
30. Sharma, A. Production of xylitol by catalytic hydrogenation of xylose. *Pharma Innov.* **2014**, *2*, 1–6.